Broadband measurements of the transient optical complex dielectric function of a nanoparticle/polymer composite upon ultrafast excitation

M. Kiel,[1] H. Möhwald,[2] and M. Bargheer[1,3,*]

[1]*Institute of Physics and Astronomy, University Potsdam, Karl-Liebknecht-Strasse 24-25, D-14476 Potsdam, Germany*

[2]*Max-Planck-Institute of Colloids and Interfaces, D-14476 Potsdam, Germany*

[3]*Helmholtz Centre, Albert-Einstein-Strasse 15, D-12489 Berlin, Germany*

(Received 11 April 2011; revised manuscript received 30 May 2011; published 24 October 2011)

We determined experimentally the complex transient optical dielectric function of a well-characterized polyelectrolyte/gold-nanoparticle composite system over a broad spectral range upon short pulse laser excitation by simultaneously measuring the time-dependent reflectance and transmittance of white light pulses with femtosecond pump-probe spectroscopy. We extracted directly the ultrafast changes in the real and imaginary parts of the effective dielectric function, $\epsilon_r^{\mathrm{eff}}(\omega,t)$ and $\epsilon_i^{\mathrm{eff}}(\omega,t)$, from the experiment. This complete experimental set of information on the time-dependent complex dielectric function challenges theories modeling the transient dielectric function of gold particles and the effective medium.

DOI: 10.1103/PhysRevB.84.165121 PACS number(s): 78.67.Bf, 78.47.J−, 78.20.N−

The dielectric function of a material is the fundamental parameter for understanding and predicting the interaction of electromagnetic waves with the material. For composite materials with nanoscale enclosures, the wavelength of optical light is much larger than the spatial variation of the dielectric function, and the interaction can be described by an effective dielectric function. For applications such as communication using nano-optical components[1–3] or various optical sensors,[4–8] it is essential to understand the transient changes of the dielectric function on ultrafast time scales, and from the viewpoint of fundamental science it is interesting to see how the nanoscale tailoring leads to particular phenomena.

Depending on the shape, size, and density of the composite constituents, different theories are used to predict the steady-state effective dielectric function from the known dielectric functions of the constituent materials.[9,10] Particularly well studied systems are gold films and nanoparticles, on which many experiments using ultrafast excitation have been performed.[11–18] The transient complex dielectric constant for a particular wavelength was deduced from measurements of the transmittance T and reflectance R in gold films[16] and in gold nanorods from optical heterodyne four-wave-mixing spectroscopy.[19] For Au particles, the complex dielectric function was experimentally determined for a laser-induced temperature change, however without accounting for the time dependence.[17] The standard tool for measuring the static dielectric function of thin films is spectroscopic ellipsometry, although its application in the ultrafast time domain is experimentally challenging.[20]

Although several papers report on ultrafast experiments for different wavelengths either in reflection or transmission geometry[11–15,17,18,21] and there is a large body of literature on the calculation of the transient response, there is no complete experimental account of the transient effective dielectric function over a broad spectral range for nanoparticle composites.

The standard way of predicting the ultrafast optical response of the composite is to calculate how the rapid rise in electron temperature smears out the Fermi edge of gold after relaxation of the nonequilibrium electron distribution.[11,12,14,22] From this, the transient imaginary part of the bulk dielectric function of gold $\epsilon_i^{\mathrm{Au}}(\omega,t)$ is determined from a band-structure model, and subsequently the real part $\epsilon_r^{\mathrm{Au}}(\omega,t)$ is deduced by a Kramers-Kronig analysis. An effective-medium theory (such as Maxwell-Garnett) then derives the transient complex dielectric function $\epsilon^{\mathrm{eff}}(\omega,t)$, where both the real and imaginary parts contain information on the physical processes of exciting the electrons in gold. Despite the large body of literature, these standard theories have only partially been tested against experiments, mainly because a set of consistent experimental information was missing.

In this paper, we determine directly the time-dependent effective dielectric function $\epsilon^{\mathrm{eff}}(\omega,t)$ of a polyelectrolyte/gold-nanoparticle compound system upon excitation from simultaneous measurements of the transient reflectance and transmittance of the sample with a time resolution of 200 fs. From the measured $T(\omega,t)$ and $R(\omega,t)$, we find values of the real and imaginary parts, $\epsilon_r^{\mathrm{eff}}(\omega,t)$ and $\epsilon_i^{\mathrm{eff}}(\omega,t)$, using textbook equations for describing reflectances and transmittances of thin films.[23] All input parameters are determined experimentally. Simulations can now focus on the calculation of the imaginary part of the effective dielectric function that is directly comparable to the experimental values of $\epsilon_i^{\mathrm{eff}}$, so that Kramers-Kronig extrapolation for $\epsilon_r^{\mathrm{eff}}$ is redundant. This experimental procedure yields an excellent testing ground for developing theories that take into account all necessary processes that influence the effective dielectric function of a nanocomposite on the ultrafast time scale.

I. EXPERIMENT

Time-resolved optical pump-probe experiments were performed with a regeneratively amplified Ti:sapphire laser system from Spectra-Physics (MaiTai/Spitfire Pro). It provides 140 fs pulses of 0.3 mJ at a repetition rate of 5 kHz and at a center wavelength of 795 nm. A small fraction of approximately 10 μJ are frequency-doubled in a BBO crystal and focused onto the sample with a pump fluence of about 5 mJ/cm^2 at 400 nm. Another 2 μJ of the laser energy are used to generate a white light continuum in a 1-mm-thick sapphire plate. This light is used for probing the sample after

excitation and is recorded simultaneously in transmission and reflection geometry with a two-channel fiber spectrometer (Avantes). Since the sample exhibits a multilayer structure (described below), we use an s-polarized probe beam such that the measured dielectric function becomes independent of the angle of incidence and to circumvent complications due to potential birefringence. In order to maximize the deposited energy in the sample, the pump beam is p-polarized. The time delay t between the pump and probe beam is regulated by a computer-controlled mechanical delay stage. A chopper in the optical pump path allows for rapid multiple determination of the relative changes of the reflectance $\Delta R(\omega,t) = \frac{R(\omega,t)-R_0(\omega)}{R_0(\omega)}$ and transmittance $\Delta T(\omega,t) = \frac{T(\omega,t)-T_0(\omega)}{T_0(\omega)}$ by measuring the perturbed and unperturbed sample with a chopping rate of 20 Hz. Here $R_0(\omega)$ and $T_0(\omega)$ are the static reflectance and transmittance of the sample. We investigate a multilayered sample that is composed of gold nanoparticles (Au-NP) in a polyelectrolyte medium of poly(sodium 4-styrenesulfonate) (PSS) and poly(allylamine hydrochloride) (PAH). The spherical nanoparticles measure 10 nm in diameter and were purchased from Sigma-Aldrich in an aqueous solution. The sample was deposited on a microscopic soda-lime glass slide by the layer-by-layer (dip coating) technique and has the following layering sequence: PEI[$(PSS/PAH)_{10}$ Au-NP/PAH]$_4$. The PSS/PAH double layers guarantee a clear separation of the particles, and clustering is avoided, although the filling factor of $f = \frac{\text{volume}_{\text{Au}}}{\text{volume}_{\text{tot}}} = 4\%$ is rather large. We characterized the sample thoroughly by x-ray reflectometry (XRR), transmission electron microscopy (TEM), atomic force microscopy (AFM), and optical spectroscopy in the same way as presented previously for analogous spin-coated samples.[24] In particular, AFM images clearly show only rare occasions of in-plane clustering of the particles, while XRR proves the clear separation of the individual layers. Since each layer is much thinner (≈20 nm) than the optical wavelength, we treat the sample as a single layer with an effective dielectric function ϵ^{eff}.

The static transmittance and reflectance of the sample and of a plain reference substrate are carefully examined at an incidence angle of 0°. Small diffuse scattering contributions to the transmitted and reflected signal are measured separately using an integrating sphere. Its total amount $(R + T)$ varies between 10^{-4} and 10^{-3} over the whole spectral range. The static dielectric functions of the substrate and the sample are derived independently from these measurements. Figure 1 shows the transmittance and reflectance of the sample (left axis) and the corresponding calculated dielectric function of the effective medium (right axis).

The time-resolved pump-probe experiments are performed at an angle of incidence of $\alpha = 40°$ for which R_0 and T_0 were calculated from the measured dielectric function shown in Fig. 1. These values are in good agreement with static cross-check measurements at this angle using a HeNe-laser (543 nm) that yield $R_0 = 0.15$ and $T_0 = 0.52$. Note that at $\alpha = 40°$, the reflection from the backside of the glass substrate can easily be separated from the reflection of the nanolayers, which is important since the observed transmittance and reflectance are altered if these beam profiles overlap in space and time on the detector.

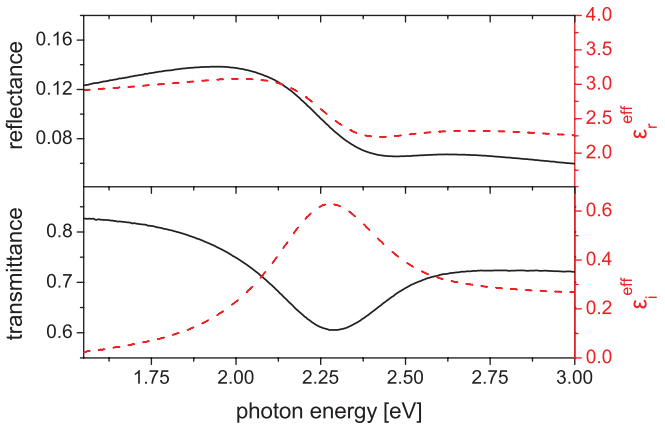

FIG. 1. (Color online) Transmittance and reflectance spectra at normal incidence (black solid lines) together with the real and imaginary parts of the static dielectric function (red dashed lines) derived from these measurements.

II. TRANSIENT REFLECTANCE AND TRANSMITTANCE

The color-coded contour plots in Figs. 2(b) and 2(c) present the simultaneously recorded transient reflectance and transmittance with probe wavelengths (energies) ranging from 445 nm (2.79 eV) to 790 nm (1.57 eV). Figures 2(a) and 2(d) show temporal profiles from horizontal cuts in the contour plots for three photon energies of 2.06, 2.28, and 2.48 eV. Figures 2(e) and 2(f) show vertical cuts, i.e., transient reflectance and transmittance spectra for three different times (1, 3, and 5 ps). Interestingly, there is no transmittance change at 2.48 eV over the measured time range, although the reflectivity changes by ∼14%. Thus, the absorption decrease must exactly balance the increased reflectance.

The observed spectral features in the transmittance change are in excellent agreement with transient transmittance data from the literature.[11,25] Comparison to the literature allows for qualitative assignment of several observed structures: The rise time of ∼500 fs is attributed to the relaxation of the nonequilibrium electron distribution to a hot Fermi distribution.[13,22] The ∼5 ps decay constant corresponds to the time it takes the electron-phonon system to equilibrate under strong excitation conditions.[16,26] The transient deviates strongly from single exponential behavior as the heat capacity of the electron system and electron-phonon coupling depend on the electron temperature.[26,27] The most remarkable feature in Fig. 2(c) is the time-independent spectral position of the zero node in the transmittance at 2.48 eV, while the second zero node shifts from 2.06 to 2.17 eV, showing an abrupt end of the shifting after 7 ps.

III. TRANSIENT DIELECTRIC FUNCTION

In order to discuss the physical phenomena leading to the observed changes, and especially as a benchmark for a full theoretical description, we now derive the effective complex dielectric function, since this is the quantity that will be calculated from any physical theory. Naively, one might expect that the transmittance change is dominated by a change of the imaginary part of the effective dielectric

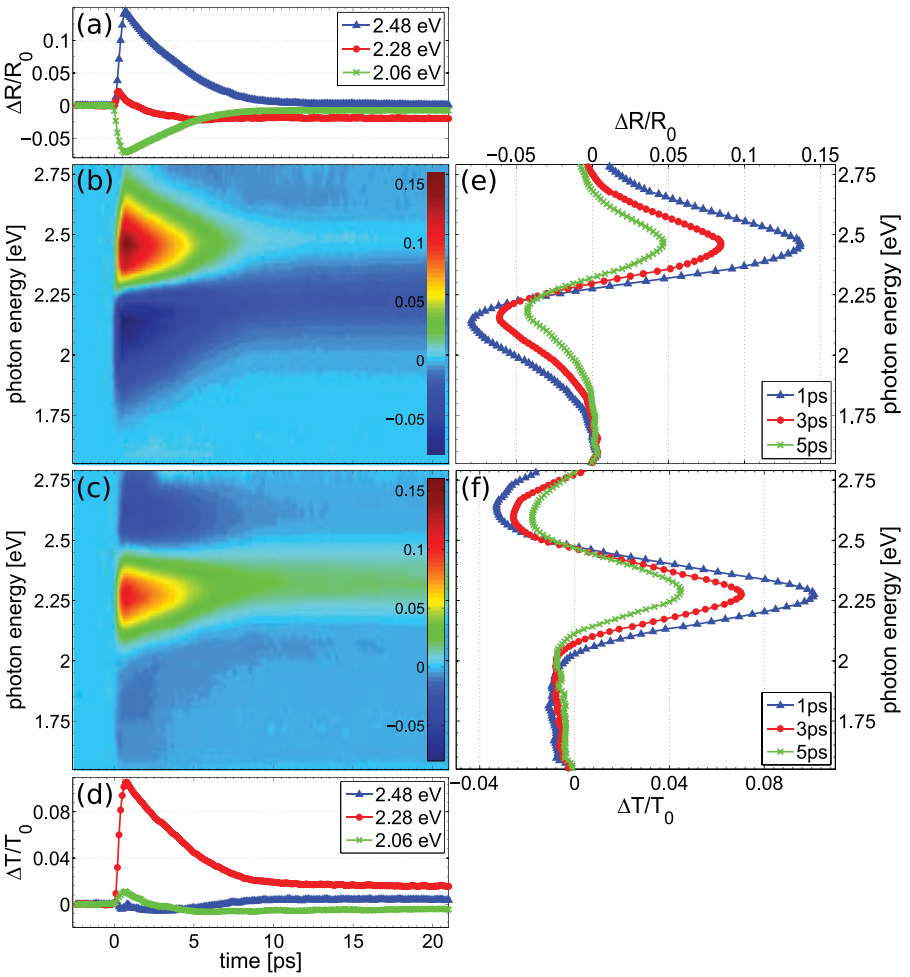

FIG. 2. (Color) The contour plots (b) and (c) show the simultaneously measured transient spectra of the reflectance and transmittance, respectively. Transient changes of reflectance (a) and transmittance (d) for three single energies from horizontal cuts through (b) and (c). Three difference spectra [vertical cuts through (b) and (c)] are presented in panels (e) and (f).

function which is responsible for the absorption coefficient $\alpha = \frac{\omega}{c_0 n}\epsilon_i$ in Lambert-Beer's law. However, the real part of the refractive index n in the denominator depends on ϵ_r and ϵ_i via $n = \sqrt{(\epsilon_r + |\epsilon|)/2}$. Moreover, the transmittance depends on the reflectance change as well ($\Delta T = -(\Delta A + \Delta R)$), and R can contain a complex wavelength-dependent interference of the nanolayer. While for an optical system of air/layer/air the resulting equations are still rather simple, the typical situation air/layer/substrate/air can only be solved numerically.

The direct correspondence of the dielectric function with the measurable quantities is[16–18,22]

$$\frac{\Delta R}{R} = r_1 \Delta\epsilon_1 + r_2 \Delta\epsilon_2, \tag{1}$$

$$\frac{\Delta T}{T} = t_1 \Delta\epsilon_1 + t_2 \Delta\epsilon_2. \tag{2}$$

The parameters $r_i = \frac{\partial \ln R}{\partial \epsilon_i}$ and $t_i = \frac{\partial \ln T}{\partial \epsilon_i}$ are given by the dielectric functions of the film and the substrate and by geometrical parameters as the angle of incidence and layer thickness.[16–18,22] The reverse problem, to infer the complex dielectric function from the measurement of reflectance and transmittance, cannot be given in closed form, and multiple solutions are mathematically possible.

To find the physically correct solution of the problem, we resorted to the following procedure: For a reasonable range of the real (ϵ_r^{eff}) and imaginary (ϵ_i^{eff}) parts of the dielectric function describing the nanolayer, we calculated the amplitudes of the reflected (ρ) and transmitted (τ) fields for any possible combination of these input values using a matrix formalism for plane-parallel multilayers.[23,28] Additional input parameters were determined experimentally: the angle of incidence, the static dielectric function of the substrate, and the thickness of the effective medium, which had been determined by XRR. The reflectance $R \propto |\rho|^2$ is simple to calculate, as we blocked the reflection from the substrate/air interface in the measurement. However, the transmittance requires us to take into account the substrate/air reflection appropriately. From this procedure, we obtain the reflectance change $\Delta R(\epsilon_r^{\text{eff}}, \epsilon_i^{\text{eff}})$ and the transmittance change $\Delta T(\epsilon_r^{\text{eff}}, \epsilon_i^{\text{eff}})$, respectively, which are illustrated by the contour plots in Fig. 3, corresponding to a probe wavelength of 543 nm. The calculation has to be repeated for each probe wavelength.

The intersection of the contour lines corresponding to the measured ΔR and ΔT is found numerically, thus identifying the real and imaginary part of ϵ_{eff} for all wavelengths and for any measured point in time. If the contour lines intersect at a large angle, as is shown in Fig. 3, the inversion yields precise results. If the contour lines for $\Delta R(\epsilon_r^{\text{eff}}, \epsilon_i^{\text{eff}})$ and $\Delta T(\epsilon_r^{\text{eff}}, \epsilon_i^{\text{eff}})$ are rather parallel for the measured values, the error of finding the intersection point increases.

With this procedure, the time-dependent dielectric function is determined directly from simultaneous measurements of the

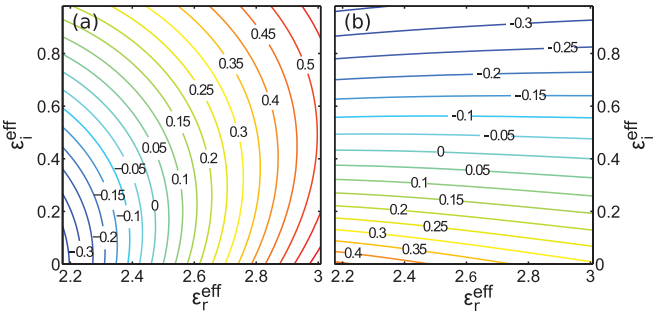

FIG. 3. (Color online) Calculated change in (a) reflectance and (b) transmittance at 543 nm for the assumed sets of values of the real and imaginary parts of the effective dielectric function. The functions $\Delta R(\epsilon_r^{\text{eff}},\epsilon_i^{\text{eff}})$ and $\Delta T(\epsilon_r^{\text{eff}},\epsilon_i^{\text{eff}})$ are calculated individually for each probe-wavelength.

reflectance and transmittance. Note that the calculated contour plots in Fig. 3 are *not* specific to the effective medium. The only input assumptions are the precisely measured layer thickness and the measured optical properties of the substrate.

The transient dielectric function for wavelengths ranging from 445 nm (2.79 eV) to 790 nm (1.57 eV) in the measured time interval is plotted in Fig. 4. Again, three spectral profiles at 1, 3, and 5 ps are plotted as well as the spectral cuts at 2.06, 2.28, and 2.48 eV.

The spectral profiles in Figs. 4(e) and 4(f) reveal that the changes in ϵ_r^{eff} and ϵ_i^{eff} conform qualitatively to $\Delta R(\omega)$ and $\Delta T(\omega)$. This is not necessarily expected, as the relationship is not linear. For a gold-particle/glass nanocomposite, the four coefficients $r_{1,2}(\omega)$ and $t_{1,2}(\omega)$ from Eqs. (1) and (2) were found to have a pronounced wavelength dependence.[22] We follow this evaluation scheme and plot the calculated coefficients in Fig. 5. In our case, the imaginary part of the dielectric function dominates the transient transmittance over the whole spectral range ($|t_2| \gg |t_1|$), even across the resonances. In contrast, the contribution of the imaginary part to the reflectance (r_2) increases rapidly above 2.2 eV. Having noted this, we can compare the contour plots in Figs. 4 and 2 again and notice that in fact the transient transmittance change is very similar to the transient changes in the imaginary part of the dielectric functions [panels (c) of both figures], whereas the transient reflectivity clearly shows a different shape above 2.2 eV compared to the real part of the dielectric function [panels (b)].

IV. DISCUSSION

We have determined experimentally all parameters needed for a precise determination of the transient dielectric function. We believe that this complete set of information will simplify the comparison to physical theories describing the mechanisms for transient changes of the dielectric function, and especially for detailed simulations. This facilitates connecting theory and experiment, since all the experimental details, such as the layer thickness, the dielectric function of the substrate, and the angle of incidence, have been eliminated by our evaluation, and

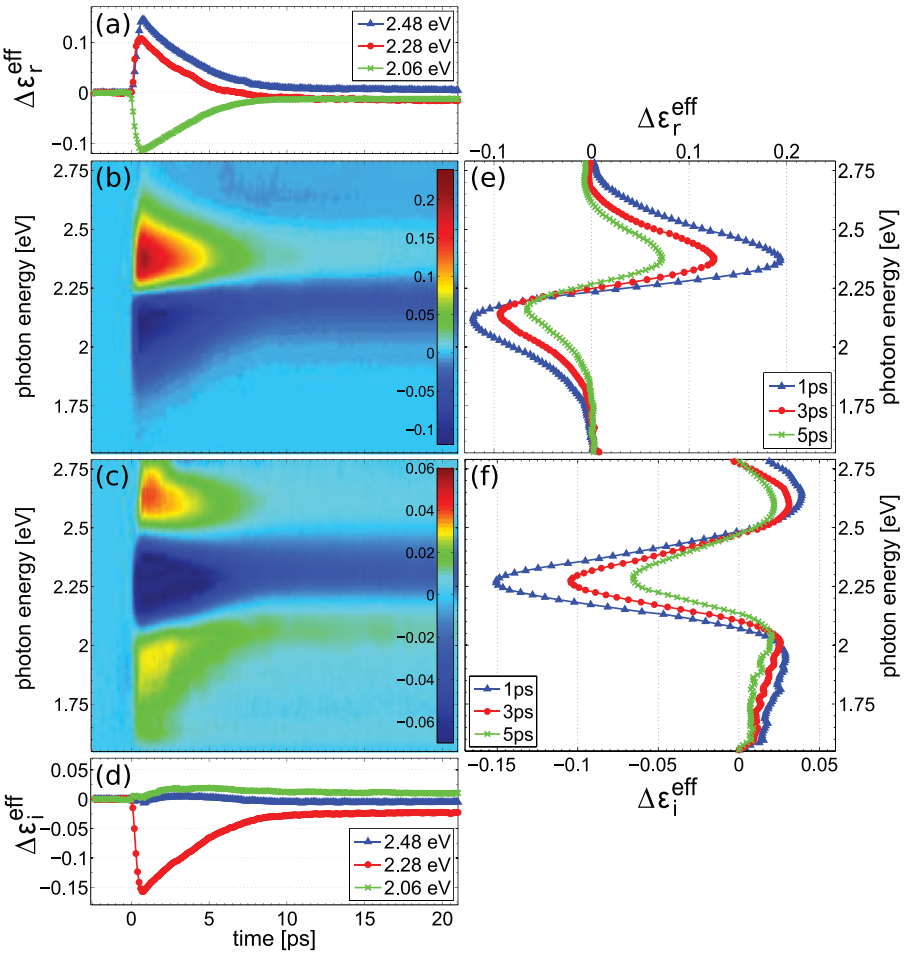

FIG. 4. (Color) Transient complex dielectric function determined from simultaneous measurements of the reflectance and transmittance. Temporal and spectral projections are again chosen for 2.06, 2.28, and 2.48 eV and for 1, 3, and 5 ps after excitation.

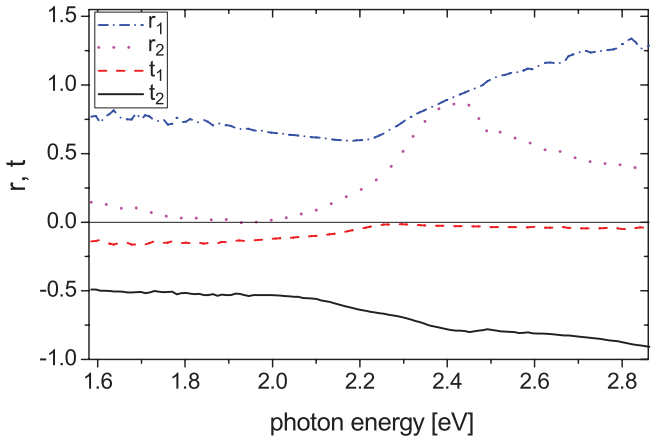

FIG. 5. (Color online) Coefficients $r_{1,2}(\omega)$ and $t_{1,2}(\omega)$ from Eqs. (1) and (2) determined from Figs. 2 and 4. These coefficients yield an excellent match for all delay times simultaneously.

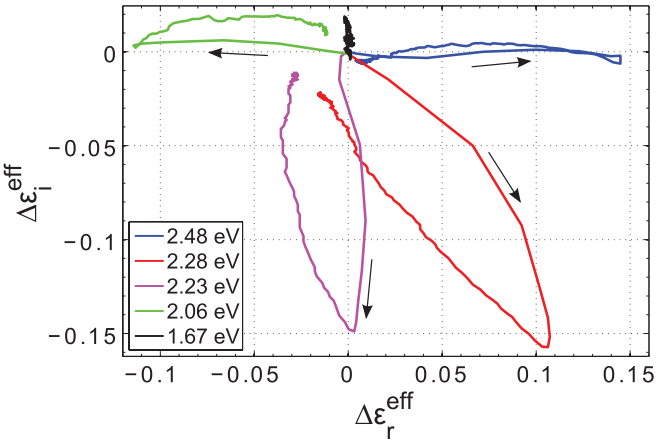

FIG. 6. (Color online) Trajectories of the complex dielectric function at five selected spectral positions. They show the different evolution of changes in the real and imaginary parts after laser-induced heating of the gold particles.

theory can focus entirely on the calculation of the dielectric function. Since we have not used Kramers-Kronig analysis to determine the complex dielectric function, theories now have to match both the transient real and imaginary parts of the dielectric function simultaneously without adjustable experimental parameters. In preliminary calculations that apply Maxwell-Garnett effective-medium theory and that follow the generally accepted theory described in the introduction, which predicts the smearing of the edge to be the dominant mechanism for the observed transmittance changes, we were able to either match the transmittance change or the reflectance change well, but a simultaneous fit to both T and R was impossible. For a full description, these theories will have to be refined.

As a summary of the observed changes, we have plotted five characteristic trajectories in Fig. 6 showing the temporal sequence of changes in the complex dielectric function for different energies around the plasmon resonance. This plot illustrates once more the quantitative differences in the changes of the real and imaginary parts of the dielectric function for different wavelengths. At 2.48 eV only the real part is changing, while at 1.67 eV we find a trajectory that only changes the imaginary part. This relatively small change in the imaginary part is in fact a rather large relative change of 27% because the static imaginary part is very small at 1.67 eV. This spectral position is probably far enough below the interband transition and should be sensitive to changes in the intraband contribution to the dielectric function (Drude part) from conduction-band electrons. The trajectories at intermediate energies show a combination of changes in the real and imaginary parts. We can identify spectral positions where the purely electronic initial changes only affect either the real part (2.06 eV) or the imaginary part (2.23 eV). Having reached the maximum change, however, the system also changes in the respective orthogonal coordinate, probably connected to the onset of the electron-phonon coupling.

V. CONCLUSION

We measured experimentally the transient complex effective dielectric function of a nanocomposite by simultaneously measuring the reflectance and transmittance of ultrashort s-polarized white light probe pulses. The results serve as a benchmark for checking theories that describe ultrafast changes of the dielectric function of nanocomposites. Such theories have to account for the changes of the particle's dielectric function and the changes in the embedding medium, such as temperature and strain variations. For the presented experiments, we have carefully measured all relevant parameters, such as the particle size and the filling factor, and we verified that clustering is avoided. The data represent an experimental challenge for theory to use an appropriate effective-medium model and gold particle dielectric function in order to obtain agreement with our derived effective dielectric constant. A detailed analysis of how the transient dielectric function of gold nanoparticles themselves can be deduced from the presented data by inverting an effective-medium formula will be given elsewhere.

ACKNOWLEDGMENT

We gratefully acknowledge the financial support by the DFG for supporting the project via BA 2281/3-1.

*bargheer@uni-potsdam.de

[1]S. Mittler, in *Optical Guided-wave Chemical and Biosensors I*, edited by O. S. Wolfbeis, M. Zourob, and A. Lakhtakia, Vol. 7 of *Springer Series on Chemical Sensors and Biosensors* (Springer, Berlin, 2009), pp. 209–229.

[2]K.-Y. Jung, F. L. Teixeira, and R. M. Reano, J. Lightwave Technol. **25**, 2757 (2007).

[3]H. Nishiyama, Y. Hirata, I. Miyamoto, and J. Nishii, Appl. Surf. Sci. **253**, 6550 (2007).

[4]J. N. Anker, W. P. Hall, O. Lyandres, N. C. Shah, J. Zhao, and R. P. Van Duyne, Nat. Mater. **7**, 442 (2008).

[5]X. Yang, E. W. Stein, S. Ashkenazi, and L. V. Wang, Wiley Interdisciplinary Rev.: Nanomed. Nanobiotech. **1**, 360 (2009).

[6]P. Jain, X. Huang, I. El-Sayed, and M. El-Sayed, Plasmonics **2**, 107 (2007).
[7]T. A. Taton, C. A. Mirkin, and R. L. Letsinger, Science **289**, 1757 (2000).
[8]T. Vossmeyer, B. Guse, I. Besnard, R. E. Bauer, K. Müllen, and A. Yasuda, Adv. Mater. **14**, 238 (2002).
[9]U. Kreibig and M. Vollmer, Optical Properties of Metal Clusters, Vol. 25 of *Springer Series in Material Science* (Springer-Verlag, Berlin, 1995).
[10]T. Ung, L. M. Liz-Marzán, and P. Mulvaney, Colloids Surf. A **202**, 119 (2002).
[11]Y. Guillet, E. Charron, and B. Palpant, Phys. Rev. B **79**, 195432 (2009).
[12]G. V. Hartland, Annu. Rev. Phys. Chem. **57**, 403 (2006).
[13]C. Voisin, D. Christofilos, P. A. Loukakos, N. Del Fatti, F. Vallée, J. Lermé, M. Gaudry, E. Cottancin, M. Pellarin, and M. Broyer, Phys. Rev. B **69**, 195416 (2004).
[14]S. Link and M. A. El-Sayed, Int. Rev. Phys. Chem. **19**, 409 (2000).
[15]S. Link and M. A. El-Sayed, Annu. Rev. Phys. Chem. **54**, 331 (2003).
[16]N. Del Fatti, C. Voisin, M. Achermann, S. Tzortzakis, D. Christofilos, and F. Vallée, Phys. Rev. B **61**, 16956 (2000).
[17]Y. Takeda, O. A. Plaksin, and N. Kishimoto, Opt. Express **15**, 6010 (2007).
[18]Y. Takeda, H. Momida, M. Ohnuma, T. Ohno, and N. Kishimoto, Opt. Express **16**, 7471 (2008).
[19]S. Park, M. Pelton, M. Liu, P. Guyot-Sionnest, and N. F. Scherer, J. Phys. Chem. C **111**, 116 (2007).
[20]M. Y. Frankel, Opt. Lett. **19**, 1252 (1994).
[21]N. Del Fatti, C. Voisin, D. Christofilos, F. Vallée, and C. Flytzanis, J. Phys. Chem. A **104**, 4321 (2000).
[22]C. K. Sun, F. Vallée, L. H. Acioli, E. P. Ippen, and J. G. Fujimoto, Phys. Rev. B **50**, 15337 (1994).
[23]M. V. Klein and T. E. Furtak, *Optik* (Springer, Berlin, 1988).
[24]M. Kiel, S. Mitzscherling, W. Leitenberger, S. Santer, B. Tiersch, T. K. Sievers, H. Möhwald, and M. Bargheer, Langmuir **26**, 18499 (2010).
[25]H. Inouye, K. Tanaka, I. Tanahashi, and K. Hirao, Phys. Rev. B **57**, 11334 (1998).
[26]G. V. Hartland, Phys. Chem. Chem. Phys. **6**, 5263 (2004).
[27]Z. Lin, L. V. Zhigilei, and V. Celli, Phys. Rev. B **77**, 075133 (2008).
[28]The formalism fully accounts for multiple reflections in plane-parallel layers, i.e., from the two sides of the effective medium. This is important, because the sample's surface roughness, which was measured by AFM to be about 2 nm, is about two orders of magnitude smaller than the wavelength of investigation, such that multiple reflections inside the sample layer add up coherently and contribute considerably.